Connexin 43 mediates spread of Ca^{2+}-dependent proinflammatory responses in lung capillaries

Kaushik Parthasarathi,[1] Hideo Ichimura,[1] Eiji Monma,[1] Jens Lindert,[1] Sadiqa Quadri,[1] Andrew Issekutz,[2] and Jahar Bhattacharya[1,3]

[1]Lung Biology Laboratory, St. Luke's–Roosevelt Hospital Center, Department of Physiology and Cellular Biophysics, College of Physicians and Surgeons, Columbia University, New York, New York, USA. [2]Departments of Pediatrics, Microbiology and Immunology, and Pathology, Dalhousie University, Halifax, Nova Scotia, Canada. [3]Department of Medicine, St. Luke's–Roosevelt Hospital Center, College of Physicians and Surgeons, Columbia University, New York, New York, USA.

Acute lung injury (ALI), which is associated with a mortality of 30–40%, is attributable to inflammation that develops rapidly across the lung's vast vascular surface, involving an entire lung or even both lungs. No specific mechanism explains this extensive inflammatory spread, probably because of the lack of approaches for detecting signal conduction in lung capillaries. Here, we addressed this question by applying the photolytic uncaging approach to induce focal increases in Ca^{2+} levels in targeted endothelial cells of alveolar capillaries. Uncaging caused Ca^{2+} levels to increase not only in the targeted cell, but also in vascular locations up to 150 μm from the target site, indicating that Ca^{2+} was conducted from the capillary to adjacent vessels. No such conduction was evident in mouse lungs lacking endothelial connexin 43 (Cx43), or in rat lungs in which we pretreated vessels with peptide inhibitors of Cx43. These findings provide the first direct evidence to our knowledge that interendothelial Ca^{2+} conduction occurs in the lung capillary bed and that Cx43-containing gap junctions mediate the conduction. A proinflammatory effect was evident in that induction of increases in Ca^{2+} levels in the capillary activated expression of the leukocyte adherence receptor P-selectin in venules. Further, peptide inhibitors of Cx43 completely blocked thrombin-induced microvascular permeability increases. Together, our findings reveal a novel role for Cx43-mediated gap junctions, namely as conduits for the spread of proinflammatory signals in the lung capillary bed. Gap junctional mechanisms require further consideration in the understanding of ALI.

Introduction

Acute lung injury (ALI), which continues to be associated with high mortality and morbidity in both infants and adults (1, 2), is attributable to severe lung inflammation that is observed in conditions such as sepsis, infection, acid aspiration, and head injury (1). The typical chest x-ray in ALI shows lung opacities, reflecting vascular and alveolar accumulation of inflammatory exudates and cells. Characteristically, the opacities develop rapidly and involve an entire lung, or even both lungs, indicating the spatial extensiveness of the inflammation. Although this inflammatory profile in ALI is well described (3), mechanisms underlying the spread of inflammation across the vast vascular surface area of the lung remain unexplained.

Although multiple mechanisms may contribute to spatial expansion of lung inflammation, the role of intercellular communication in the lung capillary bed has not received attention. Inflammatory spread in the lung may result from interendothelial communication of proinflammatory signaling intermediates, such as endothelial Ca^{2+} (4, 5). Ca^{2+}-dependent endothelial exocytosis of the leukocyte adhesion receptor P-selectin initiates inflammation by establishing leukocyte rolling on the vascular surface (6). Ca^{2+} conduction through endothelial gap junctions formed, for example, by connexin 43 (Cx43) could spread increases in Ca^{2+} levels between endothelial cells, thereby extending the inflammatory response.

Present understanding of interendothelial communication in intact vessels derives from studies in systemic arterioles. Both interendothelial and endothelial–smooth muscle communication in systemic arterioles coordinate vascular relaxation (7, 8). The communication occurs primarily through connexin-containing gap junctions. Although several endothelial connexins are expressed in systemic arterioles, deletion studies point to endothelial Cx43 and Cx40 as critical to the regulation of systemic vasoactivity (9, 10). However in contrast to arterioles, systemic capillaries and venules neither express Cx43 nor support gap junctional communication (7). Although it is known that lungs express connexins, including Cx43 (11), the existence and the pathological significance of gap junctional communication among endothelial cells of lung microvessels remain poorly understood.

Understanding of these issues has been hampered by the lack of methods for assessing intercellular communication in alveolar capillaries, which are the usual sites of inflammatory initiation in lung. Here, we addressed this difficulty by applying the photolytic uncaging technique to induce targeted increases in Ca^{2+} levels at focal regions of the alveolar capillary (12, 13). In this approach, which is widely used in vitro, cells are loaded with the Ca^{2+} cage nitrophenyl EGTA (NP-EGTA), then Ca^{2+} is released by photolytic uncaging (14), causing localized increases in Ca^{2+} levels. Below, in

Nonstandard abbreviations used: ALI, acute lung injury; Cx43, connexin 43; IP3, inositol trisphosphate; Kf, microvascular filtration coefficient; NP-EGTA, nitrophenyl EGTA; t-BHQ, 2,5-ditert-butyl hydroquinone; XeC, xestospongin C.

Conflict of interest: The authors have declared that no conflict of interest exists.

Citation for this article: *J. Clin. Invest.* **116**:2193–2200 (2006). doi:10.1172/JCI26605.

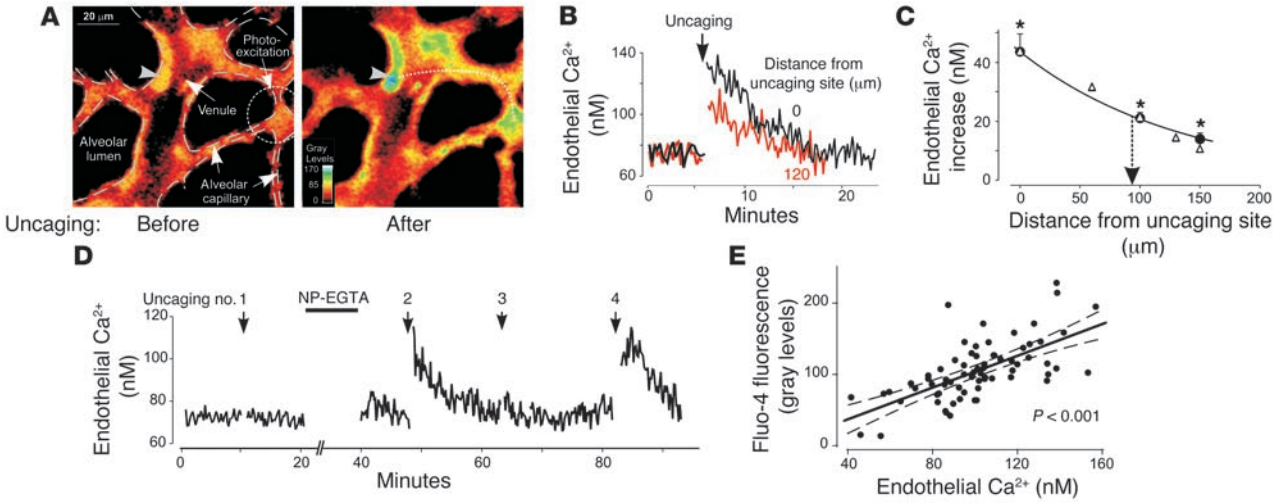

Figure 1

Photolytic uncaging-induced Ca^{2+} responses in rat lung capillaries. (**A**) Fluorescence images in pseudocolor of a rat capillary network loaded with fluo-4 and NP-EGTA show endothelial Ca^{2+} level at baseline (left) and after Ca^{2+} uncaging (right). Dashed lines and circle in baseline image represent capillary margins and uncaging target, respectively. Arrowheads indicate measurement sites on venules. The distance between measurement and uncaging sites was determined along the vascular length (dotted line). (**B**) Tracings show temporal decay of endothelial Ca^{2+} level at the uncaging site (black) and in a responding venule (red). (**C**) Filled circles represent mean Ca^{2+} responses (± SEM) to uncaging at indicated distances from the uncaging site. Each mean was higher than the baseline endothelial Ca^{2+} value (79 ± 10 nM). Line calculated by exponential regression of means ($r^2 = 0.99$). Values predicted by a computational model of diffusion (open triangles) were not significantly different from experimental values. The dashed line indicates 50% of initial. *$P < 0.05$ compared with baseline. (**D**) Tracings show responses to repeated uncaging in a capillary. As indicated, NP-EGTA was loaded after the first response (no. 1). Response nos. 1–3 were obtained at the same capillary site. Response no. 4 was obtained at a different site. The experiment was replicated 3 times. (**E**) Plot of fluo-4 fluorescence intensity against Ca^{2+} concentration determined at identical endothelial locations. Solid line calculated by linear regression ($r^2 = 0.42$). Dashed lines indicate 95% confidence intervals. Data are from 5 capillaries coloaded with fluo-4 and fura-2.

the first in situ application of the photolytic uncaging approach in an organ setting, we report findings that challenge the notion that gap junctional communication does not occur in capillaries (7). We show here that in lung capillaries, endothelial cells communicate Ca^{2+} signals through Cx43-containing gap junctions that provide a conduit for the spread of proinflammatory signals.

Results

Photoexcited Ca^{2+} uncaging. To induce physiological increases in cytosolic Ca^{2+} levels at localized vascular sites, we loaded NP-EGTA in endothelial cells lining alveolar capillaries and the first generation of postalveolar venules (Figure 1A). High-intensity UV illumination increased endothelial Ca^{2+} levels both in the targeted alveolar capillary and in venular locations lying up to 150 μm from the target (Figure 1, A and B). The evoked increases in Ca^{2+} levels decayed progressively with respect to both time and distance from the targeted site along the vascular length (Figure 1, A and B). In the reverse direction, uncaging targeted to a venule evoked increases in Ca^{2+} levels in alveolar capillaries (data not shown), indicating the presence of bidirectional Ca^{2+} conduction between the capillary and venular segments.

A plot of the mean values of the maximum increase in Ca^{2+} level against distance revealed an exponential relationship (Figure 1C). Hence, we compared exponential regressions of the experimental data and the data predicted by a diffusion-based mathematical model (Equation 1). Since 5–10 seconds elapsed between end of uncaging and beginning of imaging, we solved Equation 1 at $t = 7$ s. We estimated Q from the relations $Q = U/S$ and $U = C \times V$, where U was moles of Ca^{2+} released by uncaging and S and V were, respectively, the endothelial surface area (cm^2) and volume (cm^3) in which the uncaged Ca^{2+} was distributed by intercellular conduction. Using our experimental data, in which distance of Ca^{2+} spread was 150 μm and vessel diameter was 22 μm, we calculated an S of 10.8×10^{-5} cm^2. We estimated C as the mean Ca^{2+} concentration resulting from Ca^{2+} release at the uncaging site, namely 43×10^{-9} M. Using these values and an endothelial thickness of 0.2 μm, we calculated Q as 8.6×10^{-14} mol. The experimental and the model data indicated that the increase in Ca^{2+} level decayed to 50% of the initial value, at 94.7 and 98.5 μm from the uncaging site, respectively (Figure 1C). The similarity of these estimates suggested that the interendothelial Ca^{2+} conduction occurred by diffusion.

Since Ca^{2+} uncaging has not been carried out in lung, we conducted several experiments to rule out possible nonspecific effects. Uncaging in the absence of NP-EGTA did not increase Ca^{2+} levels (Figure 1D); hence, the present responses were not the result of nonspecific fluorophore excitation. In post-uncaged regions, a second set of photoexcitations failed to increase Ca^{2+} levels (Figure 1D), indicating that a single set of photoexcitations was sufficient to release all caged Ca^{2+} at the targeted site. However, NP-EGTA reloading allowed repeat uncaging at a specific site (data not shown), indicating that uncaging did not deteriorate the photoexcited region. In an NP-EGTA–loaded capillary, uncaging could be carried out successively at different sites (Figure 1D), indicating that a single photoexcitation did not cause nonspecific uncaging outside the targeted region. Coloading capillaries with fura-2 allowed conversion of fluorescence data for fluo-4 to units of Ca^{2+} concentration (Figure 1E).

Cx43. To define mechanisms underlying the capillary-venular Ca^{2+} conduction, we considered the role of Cx43. Since the profile

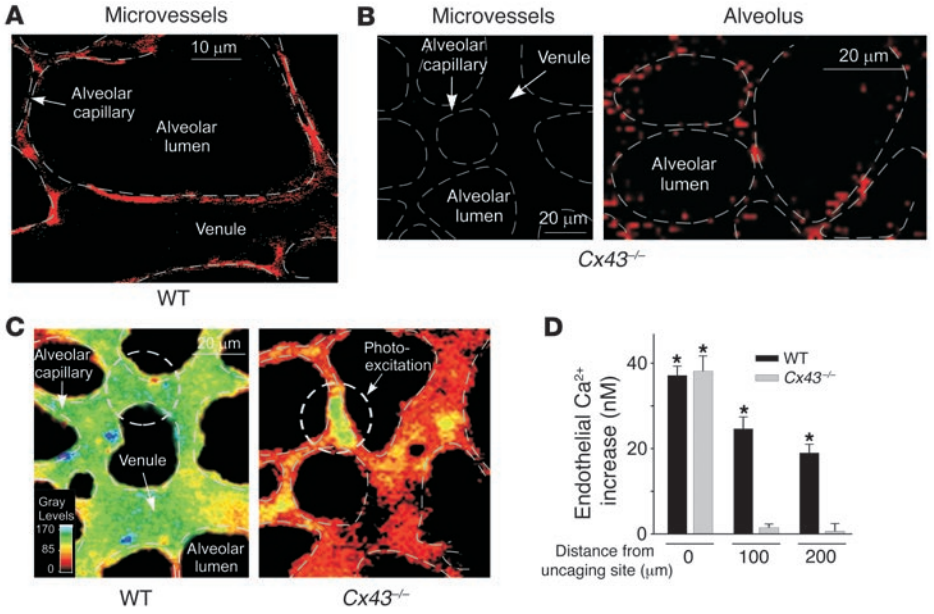

Figure 2

Distribution and functional role of Cx43 in mouse lung (WT, wild-type mice; *Cx43*$^{-/-}$, endothelium-specific Cx43-knockout mice). (**A** and **B**) Three-micrometer confocal slices of Cx43 immunofluorescence show punctuate distribution. Lines indicate capillary and alveolar margins. $n = 3$. (**C**) Pseudocolor images show endothelial fluo-4 fluorescence after Ca^{2+} uncaging. Pseudocolor was red-orange at baseline (data not shown) and changed to green after uncaging. Note that the green pseudocolor is spatially extensive in WT but localized in *Cx43*$^{-/-}$. Dashed lines and circle represent vessel margins and the uncaging target, respectively. (**D**) Group data show responses to uncaging. Baseline endothelial Ca^{2+} levels (84 ± 12 nM) were similar in the 2 groups. Mean ± SEM; $n = 3$. *$P < 0.05$ compared with baseline.

of Cx43 expression in lung microvessels is not known, we determined immunofluorescence in the alveolar capillary network using an Ab that recognizes the cytoplasmic tail of Cx43 (15–17). In WT mice, the characteristic punctate fluorescence of Cx43 (9, 18) was abundantly evident in both venules and alveolar capillaries (Figure 2A) and in alveolar epithelium (data not shown). By contrast, in mice with targeted deletion of endothelial Cx43 (*Cx43*$^{-/-}$ mice), Cx43 immunofluorescence was completely absent in the microvasculature (Figure 2B). However, direct alveolar injection of the Abs in *Cx43*$^{-/-}$ mice revealed the immunofluorescence in alveolar epithelium (Figure 2B), thereby confirming that the Cx43 deletion was endothelium specific. Control infusions of secondary Ab alone into either capillaries or alveoli did not increase fluorescence, thus excluding nonspecific staining.

In WT mice the spatial profile of uncaging-induced Ca^{2+} conduction in capillaries was similar to that in rat lungs, in that the increase in Ca^{2+} levels spread well beyond the uncaging site (Figure 2C). By contrast, in *Cx43*$^{-/-}$ mice, uncaging increased Ca^{2+} levels only at the site of photoexcitation (Figure 2, C and D). The fact that almost no Ca^{2+} spread outside the uncaging site implicated Cx43 in the Ca^{2+} conduction.

To rule out the possibility that our findings in *Cx43*$^{-/-}$ mice resulted from nonspecific effects of gene deletion, we determined responses in rat lung. The distribution patterns of Cx43 immunofluorescence in alveolar capillaries and in venules of rat lung were similar to those of mouse lung (data not shown). Studies in vitro on several cell types indicate that the peptides gap26 and gap27 ligate extracellular loops of Cx43, thereby inhibiting Cx43-dependent gap junctional communication (15, 16). Accordingly, we treated NP-EGTA–loaded capillaries with 45-minute infusions of a mixture of gap26 and gap27 (gap26/27). In these treated vessels, uncaging-induced increases in Ca^{2+} levels were localized to the targeted site (Figure 3A), indicating blockade of interendothelial Ca^{2+} conduction. Infusions of gap26 or gap27 alone also inhibited the conduction (data not shown). Washout of the peptide mixture by infusion of Ringer's solution restored the conduction (Figure 3A), indicating that the peptides did not irreversibly disable gap junctional function. In negative control assays, we determined that infusion of scrambled gap peptides failed to block Ca^{2+} conduction (Figure 3B); hence the inhibition by gap26/27 was specific. Additionally, as positive control, we determined both conducted and uncaging-induced Ca^{2+} responses in a venule during infusions of gap26/27. Gap26/27 blocked the conducted, but not the uncaging, response in the venule (Figure 3C), indicating that the lack of conducted response in the venule was specific to gap26/27. Taking our findings in mouse and rat together, we conclude that Cx43-containing endothelial gap junctions constituted the major mechanism for interendothelial Ca^{2+} conduction in lung capillaries.

Mitochondria and ER. We carried out several experiments to determine the role of Ca^{2+} uptake and release by mitochondria and ER stores in the present responses (12). These experiments indicated that mitochondrial Ca^{2+}, which was responsive to TNF-α (Figure 4A), failed to increase after uncaging (Figure 4A). To determine the role of ER stores, we treated cells with either xestospongin C (XeC), which blocks ER Ca^{2+} release (19), or 2,5-ditert-butyl hydroquinone (t-BHQ), which inhibits ER Ca^{2+} uptake (20), at concentrations that block TNF-α–induced endothelial Ca^{2+} responses, as previously reported (4). The spatial decay of the induced increase in Ca^{2+} levels was not modified by either XeC or t-BHQ (Figure 4B). In positive control assays, we determined that in XeC- and t-BHQ–loaded vessels, TNF-α–induced but not arachidonate-induced endothelial Ca^{2+} responses were blocked (data not shown). Uncaging-induced increases in Ca^{2+} levels were similar in the presence and absence of external Ca^{2+} depletion (data not shown); hence uncaging did not induce Ca^{2+} entry. These findings rule out mitochondrial or ER mechanisms as well as external Ca^{2+} as determinants of Ca^{2+} conduction from the uncaging site.

P-selectin. To determine spatial proinflammatory effects of the induced Ca^{2+} wave, we considered endothelial P-selectin expression, which denotes proinflammatory endothelial activation (4, 5). Venular P-selectin expression, which was poor under baseline conditions (4, 5), increased markedly subsequent to Ca^{2+} uncaging in an alveolar capillary (Figure 5, A and B). Infusions of second-

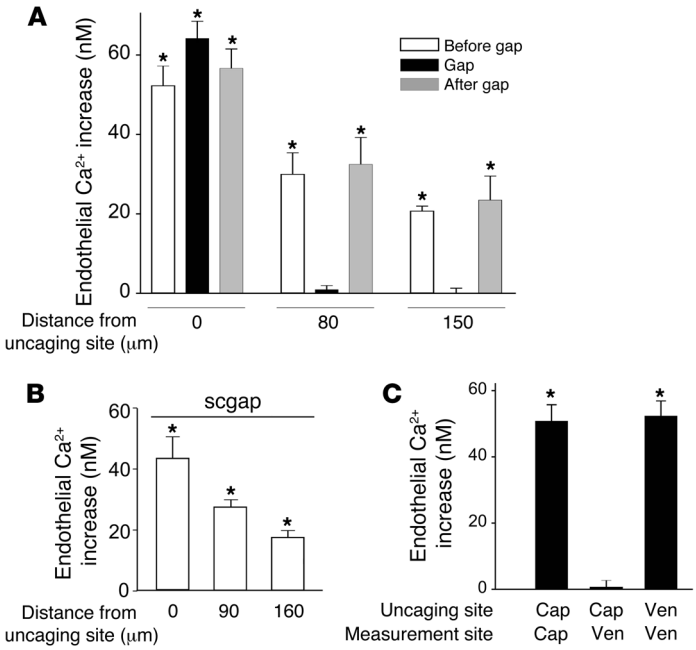

Figure 3
Inhibition of Ca^{2+} conduction in lung capillaries. Shown are responses to uncaging in alveolar capillaries, before, during (Gap), and after infusion of gap26/27. (**A** and **B**) Data show attenuation of Ca^{2+} levels with distance from uncaging site (baseline endothelial Ca^{2+} level was 76 ± 5 nM; n = 4 for each bar) and responses to scrambled gap26/27 (scgap) showing no inhibition (baseline endothelial Ca^{2+} level was 79 ± 10 nM; n = 3 for each bar). (**C**) Data show uncaging-induced responses during infusion of gap26/27 in capillaries (Cap) and venules (Ven). Capillary and venular sites were 100 μm apart. Note that the lack of venular response to capillary uncaging (second bar) was rescued by direct venular uncaging (third bar). The baseline endothelial Ca^{2+} level was 80 ± 4 nM; n = 4 for each bar. Mean ± SEM. *P < 0.05 compared with baseline.

ary Ab alone or the isotype-matched IgG did not increase fluorescence (Figure 5B), ruling out nonspecific responses. Also, no increase in P-selectin immunofluorescence was detectable in vessels of P-selectin–knockout mice (Figure 5B). In lung, P-selectin expression occurs in venules but not in alveolar capillaries (21). Accordingly, no immunofluorescence was evident at the uncaging site or in adjacent alveolar capillaries. Infusion of gap26/27, but not scrambled peptide, blocked the uncaging-induced P-selectin expression (Figure 5C). Hence, increases in Ca^{2+} levels induced in the alveolar capillary activated a proinflammatory response in the venule through Cx43-mediated communication.

Microvascular filtration coefficient. To determine the extent to which intercellular communication in lung capillaries modifies lung microvascular permeability, we quantified microvascular filtration coefficient (Kf) in isolated, blood-perfused mouse lungs. Although thrombin increased Kf in a dose-dependent manner (Figure 6A), pretreating lungs with gap26/27 completely blocked the Kf increase (Figure 6B). In contrast, scrambled gap26/27 had no effect (Figure 6B). Further, no Kf increases were detectable in P-selectin–knockout mice (Figure 6C). We interpret, that Cx43 and P-selectin each independently determined thrombin-induced increases in lung microvascular permeability.

Discussion

A central unanswered question regarding the spread of lung inflammation relates to the extent to which lung endothelial cells communicate proinflammatory signals in the alveolar capillary bed. We approached this question through determinations of Ca^{2+} conduction in lung capillaries and venules. Our findings indicate that an increase in endothelial Ca^{2+} level induced focally in an alveolar capillary evoked secondary Ca^{2+} increases in the adjacent capillary network, as well as in the adjoining venule. The secondary increases in Ca^{2+} levels were inhibited in the presence of Cx43-blocking peptides in rats, and the increases were absent in mice lacking endothelial Cx43. Further, we confirmed that Cx43 was well expressed in lung capillaries and venules of WT mice, but not in mice lacking endothelial Cx43. These findings are the first indication to our knowledge that Cx43 exists in lung capillaries and that Cx43-dependent interendothelial communication occurs in the lung capillary bed.

The potential proinflammatory significance of this communication was evident in that Ca^{2+} conduction activated venular P-selectin expression. Hence, communication from the alveolar capillary induced a proinflammatory profile in a separate vascular segment, namely in venules. Further, thrombin-induced increases in lung microvascular permeability were completely inhibited by

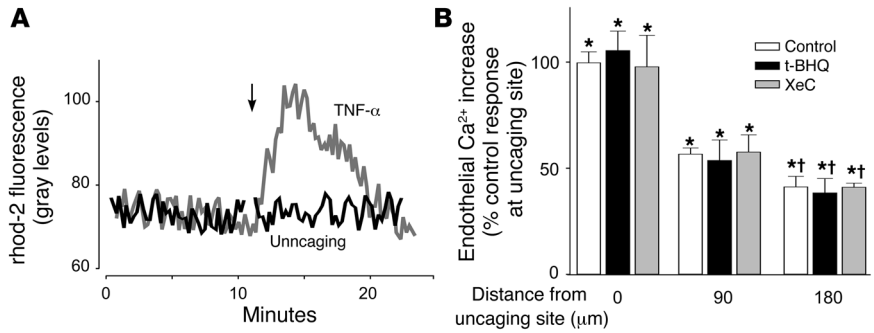

Figure 4
Role of intracellular organelles in uncaging-induced Ca^{2+} responses in rat capillaries. (**A**) Traces show mitochondrial Ca^{2+} responses in microvessels loaded with rhod-2. n = 4. (**B**) Uncaging-induced endothelial Ca^{2+} responses in capillaries and venules treated with the inhibitors t-BHQ and XeC. n = 3. The baseline Ca^{2+} level was 76 ± 10 nM. The control response at the uncaging site was an increase of 45 ± 5 nM after uncaging. Mean ± SEM; n = 3. *P < 0.05 compared with baseline. †P < 0.05 compared with respective responses at 0 μm from the uncaging site.

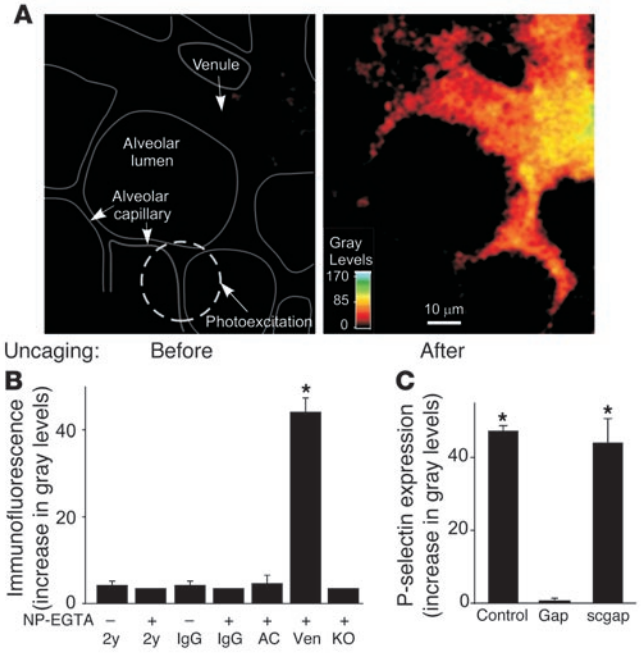

Figure 5
P-selectin expression in rat lungs. (**A**) Images show venular P-selectin immunofluorescence before (left) and after (right) uncaging. The circle and lines represent the uncaging target and vessel margins, respectively. (**B**) Group data show expression in alveolar capillaries at the uncaging site (AC) and in venules located 100 μm distant. 2y, secondary Ab only; IgG, isotype-matched IgG to P-selectin Ab; KO, P-selectin–knockout mice. Mean ± SEM. $n = 4$. *$P < 0.05$ compared with the far-left bar. (**C**) Uncaging-induced expression in the presence of gap and scrambled gap peptides. Mean ± SEM. $n = 4$. *$P < 0.05$ compared with baseline.

Cx43-blocking peptides. Increased endothelial P-selectin expression and an increase in microvascular permeability are potentially proinflammatory events, since they may underlie, respectively, leukocyte recruitment (6, 22) and lung water increase (23). Our findings indicate that such proinflammatory events are regulated by Cx43-determined mechanisms.

Ca^{2+} conduction. In cultured monolayers, increase in the Ca^{2+} level in a mechanically probed cell spreads to adjoining cells by mechanisms based on gap junctional conduction of inositol trisphosphate (IP3; ref. 12). Mechanical cell stimulation also releases ATP that exogenously ligates purinergic receptors (11), setting up paracrine mechanisms for the intercellular spread of Ca^{2+}. However, several experiments indicated that these mechanisms were not operative here. IP3-induced Ca^{2+} release from endoplasmic stores opens store-operated Ca^{2+} channels in the plasma membrane, resulting in external Ca^{2+} entry (19). However, external Ca^{2+} entry did not occur here, since the profiles of Ca^{2+} increase and the spatial decay of the induced Ca^{2+} increases were not modified by external Ca^{2+} depletion. Further, XeC, which blocks IP3-induced endoplasmic Ca^{2+} release, did not affect the evoked Ca^{2+} conduction. Moreover, inhibition of Cx43 almost completely abolished the conduction. We conclude that in contrast to the responses of mechanically stimulated cells (24), the present uncaging-induced Ca^{2+} conduction was independent of IP3, or paracrine mechanisms. To the extent that the intercommunication was bidirectional, and the experimental data matched data calculated from a model of simple diffusion, we suggest that the present gap junctional Ca^{2+} conduction was diffusive. However, this possibility requires further assessment.

Mitochondrial buffering. It is proposed that mitochondria buffer increases in the cytosolic Ca^{2+} level (25). However, here, although uncaging increased cytosolic Ca^{2+} levels, it failed to increase mitochondrial Ca^{2+} levels, indicating that mitochondrial buffering was absent. Moreover, the increases in cytosolic Ca^{2+} levels were not diminished by t-BHQ, ruling out store uptake of cage-released Ca^{2+}. In contrast to uncaging, an inducer of store release, TNF-α, caused the expected increase in mitochondrial Ca^{2+} levels (4). The mitochondrial unresponsiveness to uncaging may be due to the fact that the evoked increase in cytosolic Ca^{2+} levels occurred independently of ER mechanisms. Hence, in lung capillaries, to the extent that mechanisms of Ca^{2+} mobilization bypass the ER, mitochondrial buffering may not modify the cytosolic Ca^{2+}.

P-selectin expression. Our findings relate to the controversy surrounding the role of P-selectin in lung inflammation. Evidence against this role includes findings that P-selectin–inhibitory mAb does not block leukocyte rolling in venules (26) and that bacteria-induced leukocyte migration is not inhibited in P/E-selectin–knockout mice (27). Evidence supporting a role for P-selectin includes findings that P-selectin–blocking mAbs inhibit ALI induced by cobra venom (28) or ischemia-reperfusion (29) and that P-selectin–knockout mice are protected from ALI due to ischemia-reperfusion (30). We reported that P-selectin accounts for the pressure-induced leukocyte accumulation (6), thereby implying a role for P-selectin in the proinflammatory phenotype induced by pulmonary venous hypertension. In the present experiments, the thrombin-induced Kf increase was completely absent in P-selectin–knockout mice. Since an increase in permeability is a major feature of ALI, we believe that P-selectin might

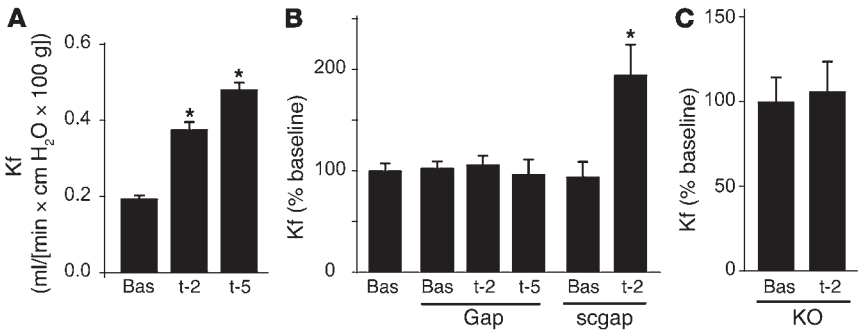

Figure 6
Thrombin-induced increase in lung microvascular permeability in mice. Thrombin doses were 2.5 (t-2) and 5.0 U/ml (t-5). Data show thrombin-induced responses at different thrombin concentrations (**A**), in gap or scrambled gap peptide–treated lungs (**B**), and in lungs of P-selectin–knockout mice (**C**). $n = 4$ for each bar in **A** and **B** and $n = 3$ for each bar in **C**. Data represent mean ± SEM. *$P < 0.05$ compared with baseline. Bas, baseline.

play a causative role in some forms of ALI. Clearly, this role needs to be better understood.

Methodological considerations. Major advantages of the present uncaging approach were that the increase in Ca^{2+} levels could be induced in a highly localized manner and that nonspecific cellular responses that might be induced by, say, mechanical stimulation were avoided. In contrast to studies using cultured cells in which photolytic uncaging occurs in submillisecond durations (13), the present uncaging required up to approximately 10 ms exposure, probably because of tissue attenuation of the uncaging UV illumination. Nevertheless, this UV exposure did not cause cell toxicity, as might be evident, say, in pericapillary edema formation or in the presence of increased cytosolic Ca^{2+} levels. Further, the capillary could be reloaded with NP-EGTA and the uncaging repeated. Hence, uncaging is an appropriate protocol for inducing physiological increases in Ca^{2+} levels in the intact lung.

Our findings address the increasing interest in connexin-mimetic peptides as tools for gap junctional studies. The lack of specific inhibitors and the early postnatal lethality of Cx43-null mice have hampered understanding (31). However, the recent availability of the connexin-mimetic peptides gap26 and gap27 provides a suitable alternative to the traditional pharmacological inhibitors (15–17). These peptides, respectively, bind the sequences VCYDKSFPISHVR and SRPTEKTIFII in extracellular loops 1 and 2 of Cx43 (15, 17), blocking gap junctional communication in several cell types (11, 15, 32). Although the mechanisms are unclear, it is suggested that the peptides inhibit cell communication by either gating or disrupting gap junction channels (11, 33, 34). Attractive features of the gap approach are that the inhibitory effect is reversible and that the mechanistic role of the specific connexin is identified. Further, the proposed extracellular sites of action rule out potential nonspecific effects attributable to cell uptake of the inhibitor (15). To the extent that our findings in lung capillaries of rat and *Cx43*$^{-/-}$ mice agree, we show that gap peptides are applicable for the in situ identification of specific connexins in lung.

In conclusion, the present evidence identifies Cx43-mediated communication as a novel mechanism that might underlie proinflammatory responses in the lung. Since the communication involves Ca^{2+} diffusion between cells, we suggest that in lung, gap junctional connections between endothelial cells provide a vascular syncytium for Ca^{2+} conduction. One consequence of this conduction was venular P-selectin expression in response to an increase in Ca^{2+} level in the alveolar capillary, which is itself incapable of P-selectin expression. Further, in the presence of thrombin, a standard permeability agonist, Cx43 inhibition blocked a 2-fold increase in lung microvascular permeability. It is possible that this inhibitory response may not be applicable under all conditions of increased lung permeability. Moreover, the extent to which intercellular communication promotes expression of other leukocyte adhesion receptors presently remains unclear. Nevertheless, our findings indicate that the role of Cx43-mediated mechanisms requires consideration in the understanding of the pathogenesis of lung inflammation underlying ALI.

Methods

Materials

Fluorophores. Fluo-4, AM (5 μM), fura-2, AM (10 μM), and rhod-2, AM (5 μM) were purchased from Invitrogen.

Agents. Cell-permeable Ca^{2+} cage NP-EGTA, AM (75 μM) was purchased from Invitrogen. Human recombinant TNF-α (100 ng/ml) (4) and thrombin (1–10 U/ml) were purchased from Sigma-Aldrich.

Abs. Mouse anti-Cx43 mAb (10 μg/ml) was purchased from Zymed; Alexa Fluor-488–conjugated goat anti-mouse Ab (5 μg/ml) was purchased from Invitrogen; and mouse anti–P-selectin mAb (RP2; 3.75 μg/ml) was used as described previously (4).

Inhibitors. Cx43 gap peptides gap26 (VCYDKSFPISHVR; 160 μM) and gap27 (SRPTEKTIFII; 190 μM) and scrambled gap peptides scgapP26 (DRYVHFSVSPICK; 160 μM) and scgap27 (SIRPETKITFI; 190 μM) were purchased from Alpha Diagnostic International. ER blockers t-BHQ (5–10 μM) and XeC (10–20 μM) were purchased from Calbiochem, EMD Biosciences.

Solutions. Agents were dissolved in HEPES-buffered vehicle with 4% dextran (70 kDa) and 1% fetal bovine serum at pH 7.4, osmolarity 295 ± 5 mOsm, and containing 150 mM Na^+, 5 mM K^+, 1 mM Ca^{2+}, 1 mM Mg^{2+}, and 10 mM glucose. To establish Ca^{2+}-free conditions, we used Ca^{2+}-free HEPES-buffered Ringer's solution containing 0.05 mM EGTA. All inhibitors were infused for 15 minutes prior to imaging, except for the gap peptides, which were infused for 45 minutes.

Animals

Animal procedures were approved by the Institutional Animal Care and Use Committee of St. Luke's–Roosevelt Hospital Center. Rats used were adult Sprague-Dawley males weighing 400–500 g. All WT mice were adult C57BL/6J males weighing 20–25 g. Vascular endothelium–specific Cx43-knockout (*Cx43*$^{-/-}$) mice on a C57BL/6J background (9) were obtained as a gift from Brian Duling, University of Virginia, Charlottesville, Virginia, USA. P-selectin–knockout mice on a C57BL/6J background were obtained from the Jackson Laboratory.

Lung preparation

Preparation of isolated blood-perfused lungs has been reported previously (4). Briefly, lungs were excised and continuously pump-perfused with autologous blood at 37°C. Final hematocrits in the perfusion were 20% and 10% for rat and mouse, respectively. The corresponding perfusion rates were 14 and 1 ml/min. Except where stated, we held pulmonary artery, left atrial, and airway pressures constant at 10, 5, and 5 cmH_2O, respectively.

Ca^{2+} imaging

We used our previously described methods (4). Briefly, we fluorescently labeled rat lung endothelial cells in situ by infusing fluorophores through a left atrial microcatheter. To label mouse endothelial cells, we directly added fluorophores into the perfusate. For wide-angle microscopy (AX70; Olympus), we detected fluorescence using an image acquisition and analysis system (CCD72, Dage-MTI; and MCID 6.0, Imaging Research). For confocal microscopy, we obtained and analyzed images using a laser scanning microscopy system (LSM 510 Meta; Zeiss).

We detected endothelial and mitochondrial Ca^{2+} using fluo-4 and rhod-2, respectively (4), at excitation and emission wavelengths of 490 and 510 nm and 545 and 565 nm, respectively. To estimate endothelial Ca^{2+} concentration, we coloaded vessels with fluo-4 and fura-2. The 340:380 emission ratio for fura-2 was used to calculate Ca^{2+} concentration (4). Codeterminations at identical capillary locations provided a calibration for estimating Ca^{2+} concentration from fluo-4 fluorescence.

Photolytic uncaging of Ca^{2+}

To load capillary endothelial cells, we infused capillaries with NP-EGTA (15 minutes). To uncage Ca^{2+}, we exposed the capillary to 8 consecutive

1-ms pulses of high-intensity (100 J) UV illumination (~320 nm) (JML-C2; Rapp OptoElectronic). The UV pulses illuminated an area 50 μm in diameter at the focal plane.

In situ immunofluorescence

We determined in situ immunofluorescence of Cx43 and P-selectin using our previously reported methods (4). Briefly, we infused the primary Ab and the fluorescence-tagged secondary Ab consecutively, and then we washed off excess Ab with Ringer's solution. For Cx43 detection, we fixed and permeabilized vessels or alveoli, prior to infusion of Abs.

Kf

Using a force transducer (BG-10; Durham Instruments), we induced weight transients to quantify Kf in isolated blood-perfused mouse lungs (35, 36). Briefly, the method entails establishing an isogravimetric (constant-weight) baseline. A step increase in left-atrial pressure by 8–9 cmH_2O is maintained for 6 minutes, causing progressive gain of lung weight. Kf is determined as the ratio of weight gain from the fourth to fifth minute to the pressure increase. We normalized Kf against wet weight of freshly isolated mouse lung (0.1424 ± 0.003 g; $n = 5$).

Mathematical model

We assumed that interendothelial Ca^{2+} conduction occurred by planar, 1-dimensional diffusion in the endothelial layer according to the Fick equation: $dC/dt = D(d^2C/dz^2)$, where C is endothelial Ca^{2+} concentration (mol/cm^3), D is the Ca^{2+} diffusion coefficient in water (8×10^{-6} cm^2/s; ref. 37), t is time (s) after uncaging, and z is distance from the uncaging site (cm). We assumed: (a) at $z = \infty$, $C = 0$; (b) at $z = 0$, $dC/dz = 0$; and (c) at $t = 0$, $C = Q \times \delta(t)$, where Q is moles per unit area (mol/cm^2) of Ca^{2+} released by uncaging, and $\delta(t)$ is the point function.

Using standard mathematical methods (38), we determined the relationship shown in Equation 1.

Equation 1

$$C(z) = \frac{Q}{\sqrt{4\pi Dt}} e^{-\left[\frac{z^2}{4Dt}\right]}$$

Statistics. All data are reported as mean ± SEM. Paired observations were compared using paired 2-tailed Student's t test or the signed-rank test. Multiple groups were compared with ANOVA (Kruskal-Wallis 1-way ANOVA on ranks), and individual paired differences among groups were determined using Dunn's or Tukey's multiple comparisons procedures. P values less than 0.05 were considered significant.

Acknowledgments

For initial studies, gap peptides were provided by Scott Boitano, University of Arizona. This project was supported by NIH grants HL75503 to K. Parthasarathi and HL57764 and HL 36024 to J. Bhattacharya.

Received for publication August 17, 2005, and accepted in revised form June 6, 2006.

Address correspondence to: Kaushik Parthasarathi, 432 West 58th Street, AJA 509, Columbia University, St. Luke's-Roosevelt Hospital Center, New York, New York 10019, USA. Phone: (212) 523-7310; Fax: (212) 523-8005; E-mail: kp257@columbia.edu.

1. MacCallum, N.S., and Evans, T.W. 2005. Epidemiology of acute lung injury. *Curr. Opin. Crit. Care.* **11**:43–49.
2. Rubenfeld, G.D., et al. 2005. Incidence and outcomes of acute lung injury. *N. Engl. J. Med.* **353**:1685–1693.
3. Ware, L.B., and Matthay, M.A. 2000. The acute respiratory distress syndrome. *N. Engl. J. Med.* **342**:1334–1349.
4. Parthasarathi, K., Ichimura, H., Quadri, S., Issekutz, A., and Bhattacharya, J. 2002. Mitochondrial reactive oxygen species regulate spatial profile of proinflammatory responses in lung venular capillaries. *J. Immunol.* **169**:7078–7086.
5. Ichimura, H., Parthasarathi, K., Quadri, S., Issekutz, A.C., and Bhattacharya, J. 2003. Mechano-oxidative coupling by mitochondria induces proinflammatory responses in lung venular capillaries. *J. Clin. Invest.* **111**:691–699. doi:10.1172/JCI200317271.
6. Ichimura, H., Parthasarathi, K., Issekutz, A.C., and Bhattacharya, J. 2005. Pressure-induced leukocyte margination in lung post-capillary venules. *Am. J. Physiol. Lung Cell. Mol. Physiol.* **289**:L407–L412.
7. Looft-Wilson, R.C., Payne, G.W., and Segal, S.S. 2004. Connexin expression and conducted vasodilation along arteriolar endothelium in mouse skeletal muscle. *J. Appl. Physiol.* **97**:1152–1158.
8. Dora, K.A., Xia, J., and Duling, B.R. 2003. Endothelial cell signaling during conducted vasomotor responses. *Am. J. Physiol. Heart Circ. Physiol.* **285**:H119–H126.
9. Liao, Y., Day, K.H., Damon, D.N., and Duling, B.R. 2001. Endothelial cell-specific knockout of connexin 43 causes hypotension and bradycardia in mice. *Proc. Natl. Acad. Sci. U. S. A.* **98**:9989–9994.
10. Figueroa, X.F., et al. 2003. Central role of connexin40 in the propagation of electrically activated vasodilation in mouse cremasteric arterioles in vivo. *Circ. Res.* **92**:793–800.
11. Isakson, B.E., Evans, W.H., and Boitano, S. 2001. Intercellular Ca2+ signaling in alveolar epithelial cells through gap junctions and by extracellular ATP. *Am. J. Physiol. Lung Cell. Mol. Physiol.* **280**:L221–L228.
12. Leybaert, L., Paemeleire, K., Strahonja, A., and Sanderson, M.J. 1998. Inositol-trisphosphate-dependent intercellular calcium signaling in and between astrocytes and endothelial cells. *Glia.* **24**:398–407.
13. Haller, T., Auktor, K., Frick, M., Mair, N., and Dietl, P. 1999. Threshold calcium levels for lamellar body exocytosis in type II pneumocytes. *Am. J. Physiol.* **277**:L893–L900.
14. Ellis-Davies, G.C., and Kaplan, J.H. 1994. Nitrophenyl-EGTA, a photolabile chelator that selectively binds Ca2+ with high affinity and releases it rapidly upon photolysis. *Proc. Natl. Acad. Sci. U. S. A.* **91**:187–191.
15. Boitano, S., and Evans, W.H. 2000. Connexin mimetic peptides reversibly inhibit Ca(2+) signaling through gap junctions in airway cells. *Am. J. Physiol. Lung Cell. Mol. Physiol.* **279**:L623–L630.
16. Chaytor, A.T., Martin, P.E., Evans, W.H., Randall, M.D., and Griffith, T.M. 1999. The endothelial component of cannabinoid-induced relaxation in rabbit mesenteric artery depends on gap junctional communication. *J. Physiol.* **520**:539–550.
17. Evans, W.H., and Boitano, S. 2001. Connexin mimetic peptides: specific inhibitors of gap-junctional intercellular communication. *Biochem. Soc. Trans.* **29**:606–612.
18. Li, W.E., Ochalski, P.A., Hertzberg, E.L., and Nagy, J.I. 1998. Immunorecognition, ultrastructure and phosphorylation status of astrocytic gap junctions and connexin43 in rat brain after cerebral focal ischaemia. *Eur. J. Neurosci.* **10**:2444–2463.
19. Schaloske, R., Schlatterer, C., and Malchow, D. 2000. A Xestospongin C-sensitive Ca(2+) store is required for cAMP-induced Ca(2+) influx and cAMP oscillations in Dictyostelium. *J. Biol. Chem.* **275**:8404–8408.
20. Pfeiffer, F., Sternfeld, L., Schmid, A., and Schulz, I. 1998. Control of Ca2+ wave propagation in mouse pancreatic acinar cells. *Am. J. Physiol.* **274**:C663–C672.
21. Feuerhake, F., Fuchsl, G., Bals, R., and Welsch, U. 1998. Expression of inducible cell adhesion molecules in the normal human lung: immunohistochemical study of their distribution in pulmonary blood vessels. *Histochem. Cell Biol.* **110**:387–394.
22. Yiming, M.T., Parthasarathi, K., Issekutz, A.C., and Bhattacharya, S. 2005. Sequence of endothelial signaling during lung expansion. *Am. J. Respir. Cell Mol. Biol.* **33**:549–554.
23. Hernandez, L.A., Coker, P.J., May, S., Thompson, A.L., and Parker, J.C. 1990. Mechanical ventilation increases microvascular permeability in oleic acid-injured lungs. *J. Appl. Physiol.* **69**:2057–2061.
24. Demer, L.L., Wortham, C.M., Dirksen, E.R., and Sanderson, M.J. 1993. Mechanical stimulation induces intercellular calcium signaling in bovine aortic endothelial cells. *Am. J. Physiol.* **264**:H2094–H2102.
25. Kaftan, E.J., Xu, T., Abercrombie, R.F., and Hille, B. 2000. Mitochondria shape hormonally induced cytoplasmic calcium oscillations and modulate exocytosis. *J. Biol. Chem.* **275**:25465–25470.
26. Gebb, S.A., et al. 1995. Sites of leukocyte sequestration in the pulmonary microcirculation. *J. Appl. Physiol.* **79**:493–497.
27. Mizgerd, J.P., et al. 1996. Selectins and neutrophil traffic: margination and Streptococcus pneumoniae-induced emigration in murine lungs. *J. Exp. Med.* **184**:639–645.
28. Mulligan, M.S., et al. 1992. Neutrophil-dependent acute lung injury. Requirement for P-selectin (GMP-140). *J. Clin. Invest.* **90**:1600–1607.
29. Moore, T.M., Khimenko, P., Adkins, W.K., Miyasaka, M., and Taylor, A.E. 1995. Adhesion molecules contribute to ischemia and reperfusion-induced injury in the isolated rat lung. *J. Appl. Physiol.* **78**:2245–2252.
30. Naka, Y., Toda, K., Kayano, K., Oz, M.C., and Pinsky, D.J. 1997. Failure to express the P-selectin gene

or P-selectin blockade confers early pulmonary protection after lung ischemia or transplantation. *Proc. Natl. Acad. Sci. U. S. A.* **94**:757–761.
31. Reaume, A.G., et al. 1995. Cardiac malformation in neonatal mice lacking connexin43. *Science.* **267**:1831–1834.
32. De Vriese, A.S., Van de Voorde, J., and Lameire, N.H. 2002. Effects of connexin-mimetic peptides on nitric oxide synthase- and cyclooxygenase-independent renal vasodilation. *Kidney Int.* **61**:177–185.
33. Chaytor, A.T., Evans, W.H., and Griffith, T.M. 1997. Peptides homologous to extracellular loop motifs of connexin 43 reversibly abolish rhythmic contractile activity in rabbit arteries. *J. Physiol.* **503**:99–110.
34. Berthoud, V.M., Beyer, E.C., and Seul, K.H. 2000. Peptide inhibitors of intercellular communication. *Am. J. Physiol. Lung Cell. Mol. Physiol.* **279**:L619–L622.
35. Safdar, Z., Yiming, M., Grunig, G., and Bhattacharya, J. 2005. Inhibition of acid-induced lung injury by hyperosmolar sucrose in rats. *Am. J. Respir. Crit. Care Med.* **172**:1002–1007.
36. Parker, J.C., Gillespie, M.N., Taylor, A.E., and Martin, S.L. 1999. Capillary filtration coefficient, vascular resistance, and compliance in isolated mouse lungs. *J. Appl. Physiol.* **87**:1421–1427.
37. Robinson, R., and Stokes, R. 1959. *Electrolyte solutions: the measurement and interpretation of conductance, chemical potential, and diffusion of simple electrolytes*. Butterworths Scientific Publications. London, United Kingdom. 571 pp.
38. Bird, R.B., Stewart, W.E., and Lightfoot, E.N. 2001. *Transport phenomena*. John Wiley and Sons. New York, New York, USA. 912 pp.